ELSEVIER

Journal of Alloys and Compounds 459 (2008) 135–141

Journal of ALLOYS AND COMPOUNDS

www.elsevier.com/locate/jallcom

On the conditions for the synthesis of bulk metallic glasses by mechanical alloying

Jatin Bhatt, B.S. Murty *

Department of Metallurgical and Materials Engineering, Indian Institute of Technology Madras, Chennai 600036, India

Received 15 February 2007; received in revised form 16 April 2007; accepted 18 April 2007
Available online 21 April 2007

Abstract

In the present study, an attempt has been made to develop milling maps/energy maps for the formation of amorphous phase in bulk glass forming alloys such as $Zr_{65}Al_{7.5}Cu_{17.5}Ni_{10}$, $Ti_{50}Cu_{23}Ni_{20}Sn_7$, $Ti_{50}Ni_{20}Cu_{20}Al_{10}$, $Cu_{60}Zr_{30}Ti_{10}$, $Fe_{56}Co_7Ni_7Zr_{10}B_{20}$, $Ni_{60}Nb_{20}Ti_{12.5}Zr_{7.5}$, $Ti_{55}Zr_{20}Ni_{25}$ and $Zr_{55}Ti_{25}Ni_{20}$. Milling parameters such as milling speed, ball to powder weight ratio have been varied over wide ranges in order to have a wide range of milling energies. The results indicate that total energy of milling has a decisive role than the impact energy of the ball in the formation of the amorphous phase by planetary ball mill. The paper compares the glass forming abilities of the various bulk glass forming compositions in terms of the milling maps in order to develop better understanding of glass forming criteria by mechanical alloying.

Keywords: Mechanical alloying; Metallic glasses; Amorphisation

1. Introduction

Bulk metallic glasses (BMGs) constitute a new exciting class of materials with unique physical and mechanical properties for structural and functional applications [1]. Various methods have been adopted to synthesize BMGs, namely, containerless processing [2], fluxing techniques to suppress heterogeneous nucleation [3] and preventing crystallization by choosing multicomponent alloys [4]. A number of multicomponent alloys exhibiting excellent glass forming ability and high stability of the glass against crystallization have been developed in recent years. In a number of multicomponent systems such as Zr [5], Ti [6], Fe [7], Cu [8], and Ni [9], cooling rates as slow as 1–100 K/s are sufficient to obtain bulk glassy samples with dimensions of several millimeters by conventional casting techniques. These alloys are sufficiently stable against crystallization to investigate the undercooled liquid state well above the glass transition temperature (T_g) and provide new insights into thermodynamics and kinetics of undercooled liquid alloys. However, the production of bulk metallic glasses by slow cooling casting techniques is still limited to narrow composition ranges, i.e., near the deep eutectics in the equilibrium phase diagram. Change in composition strongly affects the glass forming ability [10].

It is known that crystalline phases can be destabilized by disordering process that can lead to a crystal to glass transition [11]. Mechanical alloying (MA) and mechanical milling (MM) have been established over the past two decades as viable alternate routes for the synthesis of amorphous and nanocrystalline materials [12–16]. The glass forming composition range is known to be much wider in case of MA/MM than the liquid metallurgy route and is not restricted to deep eutectic compositions [13]. Murty et al. [17] and Joardar et al. [18] have shown that amorphisation and formation of intermetallics during MA is decided by the total energy imparted during milling and not the impact energy of the individual balls. Mio et al. [19] and Boytsov et al. [20] have also shown, for different materials, that total energy input is the important parameter for transformation. Abdellaoui and Gaffet [21] have also shown that neither the impact energy nor the frequency of impacts govern the amorphisation process in a planetary ball mill if taken separately but the power (which is the product of impact energy and the frequency of impacts) only is responsible for ball milled final product, which is supported also by Magini et al. [22]. Interestingly, the shock power, coined by Abdellaoui and Gaffet [21] is similar to the total energy of milling coined by Murty et al. [17], excepting that the expression of the latter includes the total number of balls, time of milling and

* Corresponding author. Tel.: +91 44 2257 4754; fax: +91 44 2257 0509.
E-mail address: murty@iitm.ac.in (B.S. Murty).

0925-8388/$ – see front matter © 2007 Elsevier B.V. All rights reserved.
doi:10.1016/j.jallcom.2007.04.242

weight of powder, in addition to the impact energy of ball and frequency of impacts. Thus, the total energy of milling includes the parameters contributing to shock power.

In the previous studies, various groups attempted to understand the phase formation during mechanical alloying in terms of milling parameters using milling maps. For example Burgio et al. [23] and Rojac et al. [24] have used ball impact energy and cumulative kinetic energy for developing a milling map. Magini et al. [22] have used power absorption and degree of filling for a milling map, while Suryanaryana et al. [25] have used ball to powder weight ratio (BPR) and milling time in a 2D milling map. Murty et al. [17] and Joardar et al. [18] have used milling map as an energy map with the impact energy of the ball and the total energy as its axes, which can delineate the energy domain of amorphisation and thus identify the conditions required for amorphisation during MA. However, so far there has been no attempt in the literature to develop milling maps for the bulk metallic glasses.

The present paper reports the attempt to synthesize amorphous phase by MA in a number of bulk metallic glass forming compositions in Zr, Ti, Fe, Cu and Ni based systems. The effect of milling parameters on the time required for amorphisation of a given composition has been studied in detail in an attempt to develop the milling maps for these compositions and to correlate the energy required for amorphisation to the glass forming ability of bulk metallic glasses.

2. Experimental details

The elemental powder blends of compositions $Zr_{65}Cu_{17.5}Ni_{10}Al_{7.5}$, $Ti_{50}Cu_{23}Ni_{20}Sn_7$, $Ti_{50}Ni_{20}Cu_{20}Al_{10}$, $Fe_{56}Co_7Ni_7Zr_{10}B_{20}$, $Ni_{60}Nb_{20}Ti_{12.5}Zr_{7.5}$, $Cu_{60}Zr_{30}Ti_{10}$, $Ti_{55}Zr_{20}Ni_{25}$ and $Zr_{55}Ti_{25}Ni_{20}$ have been mechanically alloyed in a high-energy ball mill (Fritsch Pulverisette-P5). The starting elemental powders are of −325 mesh (<45 μm) and with purity of about 99.9%. The milling had been carried out in wet condition using toluene in WC vials with WC balls of 10 mm diameter. Toluene acts as a process control agent, restricting oxidation and excessive welding of powder during milling. WC vial has an internal diameter of 75 mm and a height of 70 mm with a capacity of 250 ml. Milling was carried out at 200, 250 and 300 rpm. The linear velocity of the balls for these milling speeds was calculated [21] to be 4.80, 6.10 and 7.32 m/s, respectively. The ball to powder weight ratio is varied as 5:1, 10:1, 15:1 and 20:1 keeping the number of balls constant at 50. The experimental conditions for different compositions are shown in Table 1. Milled powder samples were taken out of the vials at regular intervals and were characterized for x-ray diffraction (XRD) using Philips X-ray diffractometer with Co Kα (λ = 0.1788 nm). The crystallite size has been calculated from the X-ray peak broadening after separation of the contributions of strain and instrumental broadening by standard procedure [26]. The alloying and amorphisation has also been monitored using a JEOL JSM scanning electron microscope (SEM). Transmission electron microscopy (TEM) was carried out on the milled samples using Philips CM12 microscope. The thermal stability of the amorphous phase has been evaluated by differential scanning calorimetry (DSC) using Netzsch DSC at a heating rate of 20 °C/min.

Table 1
Milling conditions used in the present study

Composition	$Cu_{60}Zr_{30}Ti_{10}$, $Fe_{56}Co_7Ni_7Zr_{10}B_{20}$, $Ni_{60}Nb_{20}Ti_{12.5}Zr_{7.5}$, $Ti_{50}Cu_{23}Ni_{20}Sn_7$, $Ti_{50}Ni_{20}Cu_{20}Al_{10}$, $Ti_{55}Zr_{20}Ni_{25}$, $Zr_{65}Cu_{17.5}Ni_{10}Al_{7.5}$, $Zr_{55}Ti_{25}Ni_{20}$
Milling speed (rpm)	200, 250, 300
Ball to powder weight ratio	5:1, 10:1, 15:1, 20:1

3. Results and discussion

3.1. Parametric phase diagram

Fig. 1(a) shows the XRD patterns of $Fe_{56}Co_7Ni_7Zr_{10}B_{20}$ as a function of milling time at a milling speed of 300 rpm and a ball to powder weight ratio of 5:1. With increase in milling time the XRD peaks of individual elements decrease in intensity and become broader and finally disappear leading to the formation of amorphous phase. Formation of amorphous phase has been observed after 10 h of MA for this composition under the above milling conditions. Fig. 1(b) shows the XRD patterns of the amorphous phase under different milling conditions for the above composition. Similar results have been observed for the other compositions also, except that the time required for amorphisation varied depending on the composition and milling conditions (milling speed and ball to powder weight ratio).

The time required for amorphisation (determined from the XRD patterns) in general decreased with increase in rpm and ball to powder weight ratio as shown in Fig. 2(a) and (b),

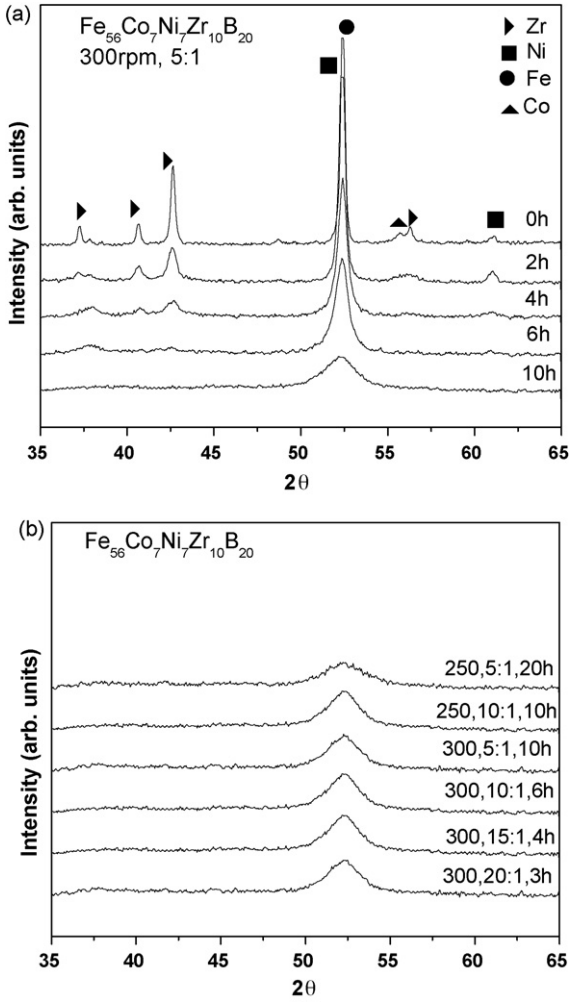

Fig. 1. XRD patterns of $Fe_{56}Co_7Ni_7Zr_{10}B_{20}$ (a) as a function of milling time at 300 rpm and 5:1 ball to powder weight ratio and (b) for the amorphous phase obtained at different rpm and ball to powder weight ratio.

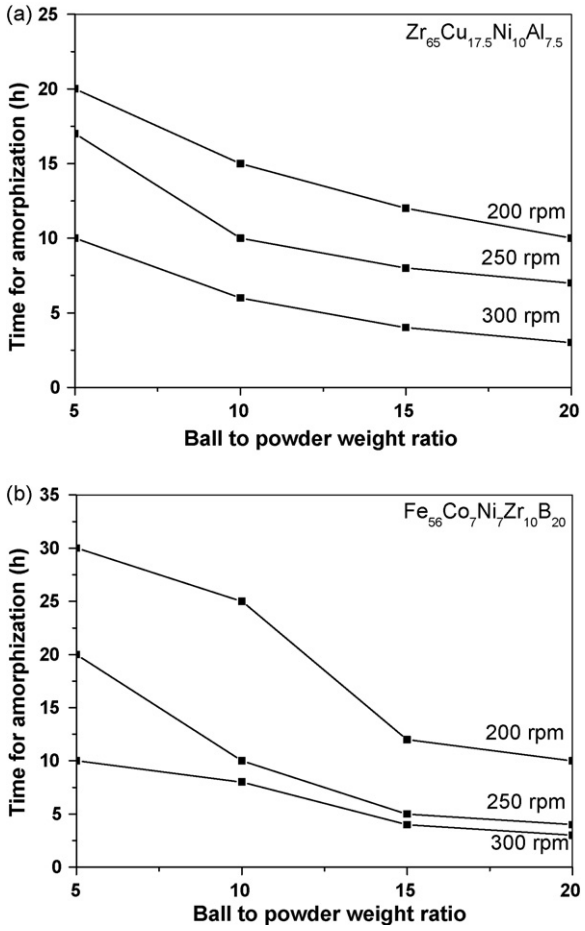

Fig. 2. Time required for amorphisation at different rpm and ball to powder weight ratio for (a) $Zr_{65}Al_{7.5}Cu_{17.5}Ni_{10}$ and (b) $Fe_{56}Co_7Ni_7Zr_{10}B_{20}$.

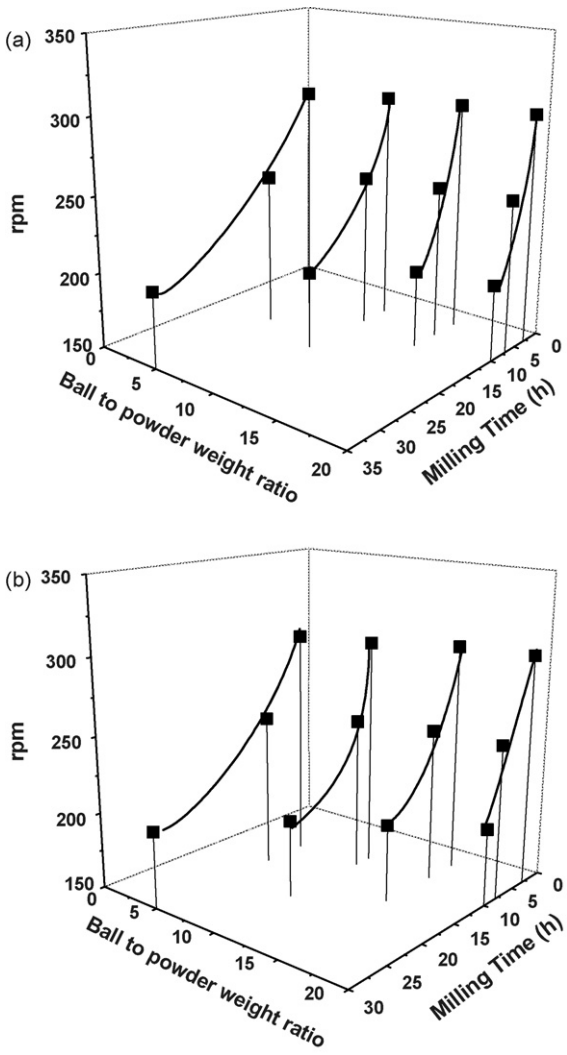

Fig. 3. Parametric phase diagrams indicating the domain of amorphous phase for (a) $Zr_{65}Al_{7.5}Cu_{17.5}Ni_{10}$ and (b) $Fe_{56}Co_7Ni_7Zr_{10}B_{20}$.

for $Zr_{65}Cu_{17.5}Ni_{10}Al_{7.5}$ and $Fe_{56}Co_7Ni_7Zr_{10}B_{20}$, respectively, which are chosen to represent all the compositions studied. Similar results were obtained by Murty and Ranganathan [13] for $Ti_{50}Ni_{50}$ and $Ti_{50}Cu_{50}$, which demonstrated that glass forming ability increases with increasing milling intensity.

Fig. 3(a) and (b) is the parametric phase diagrams giving the phase field of amorphous phase in the ternary diagram of milling speed, ball to powder weight ratio and milling time for $Zr_{65}Cu_{17.5}Ni_{10}Al_{7.5}$ and $Fe_{56}Co_7Ni_7Zr_{10}B_{20}$. The figure shows the time required for amorphisation at different combinations of milling speed and ball to powder weight ratio. It can be seen from the parametric phase diagram that slope decreases with decrease in ball to powder weight ratio from 20:1 to 5:1, irrespective of the composition studied. This suggests that at higher ball to powder weight ratio, the time required for amorphisation is not very sensitive to the milling speed, while at lower ball to powder weight ratio it is quite sensitive to the milling speed. Similar result can be observed in case of milling speed as observed in Fig. 2(b) that at higher milling speed the time required for amorphisation is less sensitive to ball to powder weight ratio. The minimum time required for amorphisation ranged between 5 and 8 h for all the compositions at 300 rpm and 10:1 ball to powder weight ratio. Fig. 4(a) and (b) shows the time required for amorphisation for different compositions as a function of ball to powder weight ratio at 300 rpm and as a function of rpm at a ball to powder weight ratio of 10:1, respectively. It is very clear that at low milling speed and ball to powder weight ratio, different compositions studied form amorphous phase over wider time frame, while at higher milling intensities (speed and ball to powder weight ratio) the time required for amorphisation is more or less the same for all the compositions.

Interestingly, the time required for amorphisation is 5 and 10 h for $Ti_{55}Zr_{20}Ni_{25}$ $Ti_{50}Cu_{23}Ni_{20}Sn_7$, which indicates faster amorphisation kinetics in the former alloy, though its Ti content is comparable with that of the latter. This could be attributed to the Zr present in the former composition, which easily dissolves in Ti (being isomorphous with Ti) and results in solid solution hardening. It is known [13] that such solid solutions become nanocrystalline faster during MA due to work hardening in comparison to pure metals. It is also known that nanocrystallization is always a prerequisite to amorphisation during mechanical alloying [13]. In case of $Ti_{50}Cu_{23}Ni_{20}Sn_7$ as the solubility of Cu, Ni and Sn in Ti are low, the crystallite size of Ti does not decrease faster, which limits the rate of amorphisation.

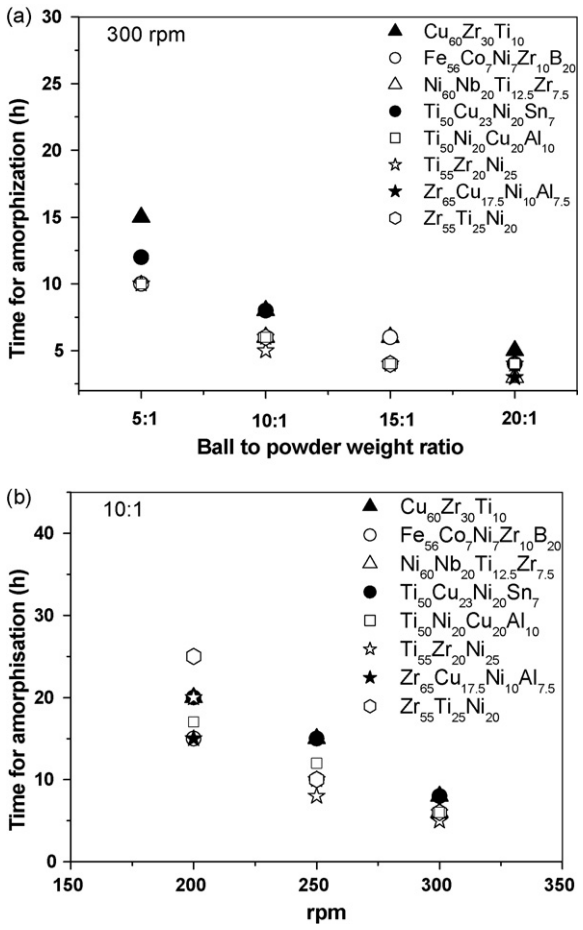

Fig. 4. Time required for amorphisation for all the compositions studied at (a) 300 rpm for different ball to powder weight ratio and (b) 10:1 for different rpm.

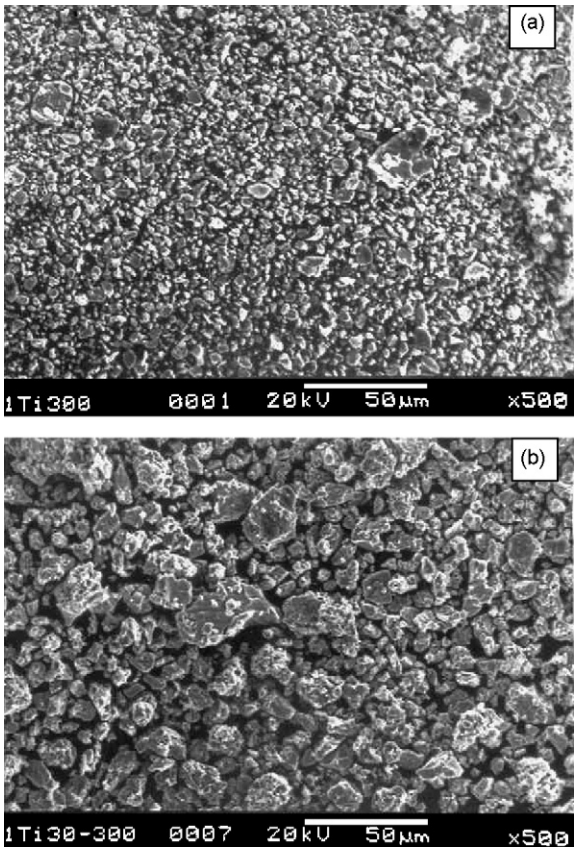

Fig. 5. SEM micrographs of $Ti_{50}Cu_{23}Ni_{20}Sn_7$ (a) just before (10 h) and (b) just after (20 h) amorphisation.

Thus, the present results (Fig. 4) indicate that the time required for amorphisation is almost the same for all the bulk metallic glass forming compositions, particularly at the higher milling intensities. This gives a clue that total energy required for the formation of amorphous phase is similar for different bulk metallic glass forming systems. This could be easily understood as the structure of amorphous phase is expected to be similar for all the bulk metallic glass forming compositions. Hence the energy required to destabilize the crystalline solid solution formed during MA is expected to be quite similar in all the bulk metallic glass forming systems.

Due to repeated fracturing and welding that occurs during mechanical alloying it results in the formation of alternate layers of pure metals powders. With the progress of milling, the particles become finer and the layer thickness decreases and finally alloying occurs when the particles become nanocrystalline. Fig. 5(a) and (b) shows the SEM photomicrographs of $Ti_{50}Cu_{23}Ni_{20}Sn_7$ elemental blend after 5 and 8 h of milling, respectively, at 300 rpm and 10:1 ball to powder weight ratio. Fig. 5(a) represents the microstructure just before amorphisation when the individual agglomerates are very fine (1–2 μm). Fig. 5(b) is the SEM micrograph after amorphisation, which indicates an increase in the particle size. This suggests excessive welding after amorphisation, which could be due to viscous flow of the amorphous phase. Similar results have been observed in all the other compositions studied. It has to be noted that the actual crystallite size is nanocrystalline and the particles seen in SEM are the agglomerates of these nanocrystallites. Under the high-energy electron beam in TEM these agglomerate get dispersed into nano-sized particles. Fig. 6 shows the TEM bright field image of the $Fe_{56}Co_7Ni_7Zr_{10}B_{20}$ alloy showing the nano-sized more or less spherical amorphous particles and the selected area

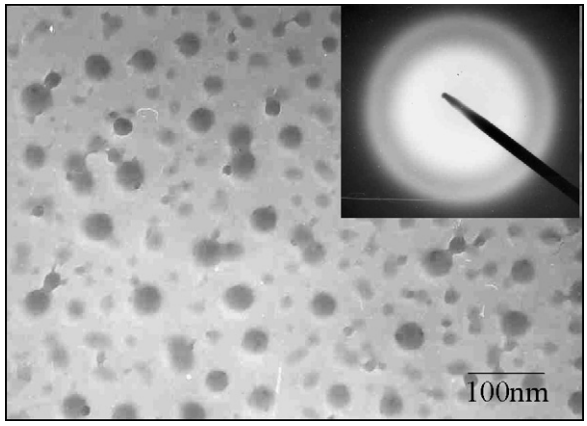

Fig. 6. TEM bright field image on $Fe_{56}Co_7Ni_7Zr_{10}B_{20}$ alloy mechanically alloyed for 10 h at the speed of 300 rpm and 5:1 ball to powder weight ratio. Inset is the selected area diffraction pattern from the particles.

diffraction pattern (inset of Fig. 6) from these particles confirms their amorphous nature.

3.2. Milling maps/energy maps

The results observed in the present study can be better understood if one considers the energy transfer during milling. Such and attempt was earlier made by Burgio et al. [23], Murty et al. [17], Joardar et al. [18] and Abdellaoui and Gaffet [21]. All the milling parameters such as type of mill, type of milling media, size of ball, number of balls, speed of the mill, ball to powder weight ratio and time of milling can be converted into two energy parameters, namely, the effective impact energy of the ball (E_b^*) and the total energy of milling (E_t) [17,18]. The milling map is a plot between E_b^* and E_t. The basic equations are given here and for details the reader is requested to refer to the early work [17,21].

The effective impact energy of the ball is given by:

$$E_b^* = \phi_b E_b = \phi_b 0.5 m_b v_b^2$$

where ϕ_b is the correction factor for different degree of filling of the vial, which is ≤ 1. For an efficient filling of the vial with milling media and powder (one third filling of the vial), the value of ϕ_b turns out to be 1. m_b and v_b are the mass and linear velocity of the ball:

$$v_b = \frac{2\pi}{60}\sqrt{\left[(R_p\Omega)^2 + (R_v - R_b)^2\omega^2\left\{1 + 2\left(\frac{\omega}{\Omega}\right)\right\}\right]}$$

where R_p, R_v and R_b are the radii of disc, vial and ball, respectively, ω and Ω are the speeds of the vial and disc, respectively.

The total energy (E_t) transferred per unit weight of powder from the balls to the system during milling is given by:

$$E_t = \frac{E_b^* n_b f_b t}{W_p}$$

where n_b is the number of balls, f_b is the frequency of impacts, t is the duration of milling and W_p is weight of powder in vial. The f_b for single ball is calculated by [27]:

$$f_b = K(\Omega - \omega)$$

where K is 1.5 for a ball diameter of 8–10 mm.

The impact energy and total energy for $Zr_{65}Cu_{17.5}Ni_{10}Al_{7.5}$ and $Fe_{56}Co_7Ni_7Zr_{10}B_{20}$ at different milling speeds and ball to powder weight ratio have been calculated according to the above formalism and are plotted in Fig. 7(a) and (b). The above plots between E_b^* and E_t can give and idea about the conditions required for amorphisation during mechanical alloying. Milling energies in excessive of that required (shown as second dashed line on the right) for the formation of amorphous phase will lead to in situ crystallization of the amorphous phase. This in situ crystallization of the amorphous phase is caused by either due to the raise in temperature during milling, or due to large number of defects generated, which can enhance the diffusivity. Thus, there is definitely an energy window, in which amorphous phase forms during MA. Similar results have been observed in all the compositions studied. The milling maps in Fig. 7 show the energy domains for amorphous phase from the elemental

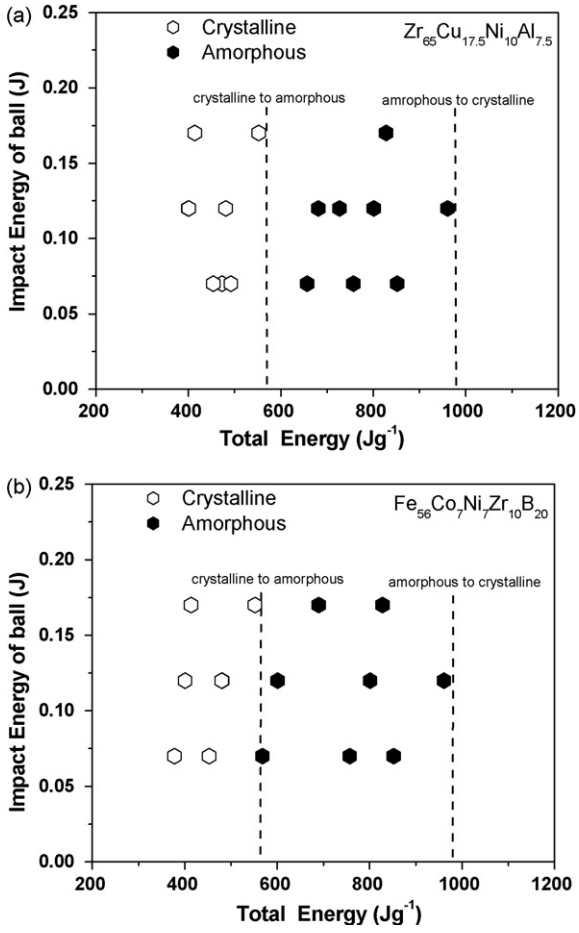

Fig. 7. Milling maps indicating the energy required for amorphisation in (a) $Zr_{65}Al_{7.5}Cu_{17.5}Ni_{10}$ and (b) $Fe_{56}Co_7Ni_7Zr_{10}B_{20}$.

blends. This map can be taken as a glass formation map that can separate out the glass forming energy regime and non-glass forming energy regime distinctly.

The milling map in Fig. 7 clearly predicts that irrespective of the E_b^*, crystal to amorphous transition occurs in a narrow E_t range of 500–600 J g^{-1} in both Zr and Fe based compositions. Interestingly, all other bulk metallic glass forming alloys studied in the present work could be amorphised at similar total energy level. The conditions of amorphisation observed in the present study could not be determined using mechanical power ($E_b^* \times f_b$) as both E_b^* and f_b remains constant for a particular rpm. In contrast, the total energy E_t clearly delineates the conditions for amorphisation as milling time is included in this parameter.It is interesting to note that the different glass forming criteria such as ΔT_x (=$T_x - T_g$, where T_x and T_g are the crystallization and glass transition temperatures of the alloys), T_{rg} (=T_g/T_l, where T_l is the liquidus temperature of the alloy) and the recently proposed γ [28], α and β [29] parameters are also quite similar for all the above highly glass forming compositions. Thus, there appears to be strong correlation between the GFA from the liquid and that during MA. Strong correlations have been observed in the present study with all the above glass forming criteria and the milling energy required for amorphisation [30]. Present milling map

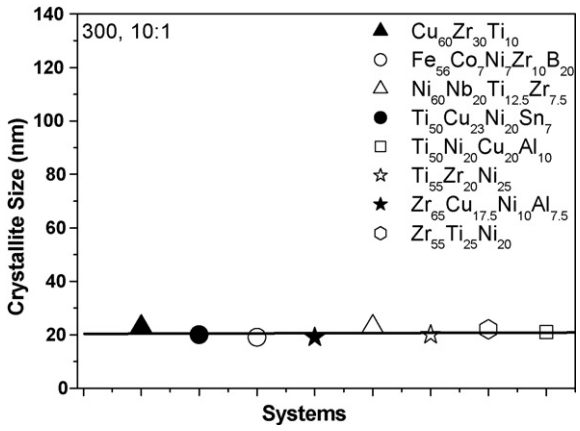

Fig. 8. Crystallite size of various systems showing nano-formation as prerequisite of amorphisation.

also suggests that there is common energy window for all the compositions in which amorphisation is seen. In addition, the present study has also shown that amorphisation occurs when the crystallite size of the solvent element reaches a critical value of about 20 nm in all the compositions studied as shown in Fig. 8.

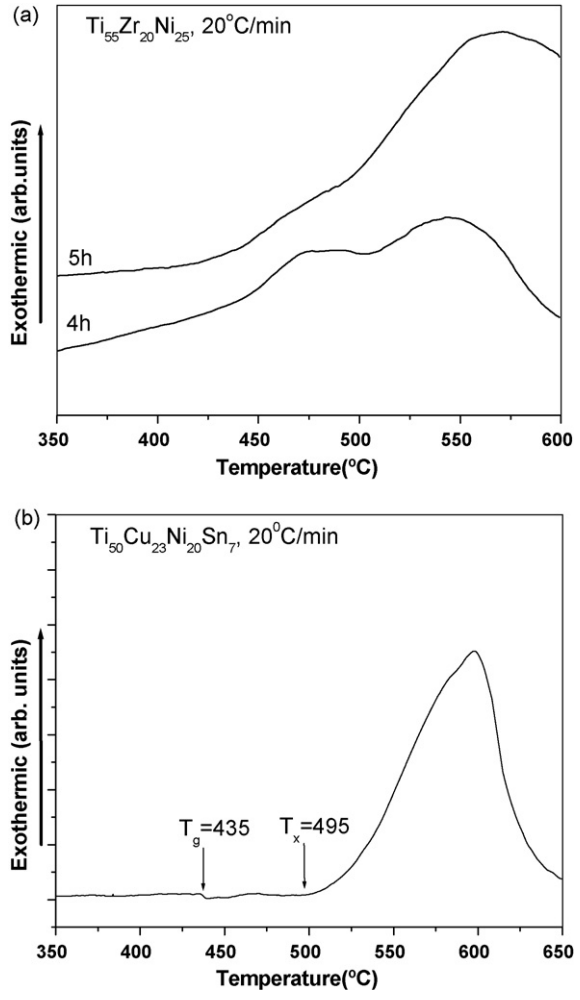

Fig. 9. DSC traces of (a) $Ti_{55}Zr_{20}Ni_{25}$ and (b) $Ti_{50}Cu_{23}Ni_{20}Sn_7$ at a heating rate of 20 °C/min.

Fig. 9(a) and (b) shows typical DSC traces for the mechanically alloyed Ti based compositions. Fig. 9(a) shows the DSC traces of $Ti_{55}Zr_{20}Ni_{25}$ after 4 and 5 h of MA at 300 rpm and 10:1 ball to powder weight ratio. For this composition, amorphisation has been observed after 5 h of MA under the above milling conditions. Interestingly, the DSC trace of the sample before amorphisation shows two exotherms, while that of the amorphous sample shows one exotherm. The first exotherm in the sample milled for 4 h can be attributed to the solid-state amorphisation of the elemental blend by the thermal activation provided during heating, while the second exotherm is due to the crystallization of the amorphous phase. Similar results were observed by Murty et al. [31] in Ti-Ni-Cu alloys. It is obvious that the amorphous sample (5 h milled) does not show the first exotherm that was observed in case of the 4 h milled sample. DSC traces of most of the compositions studied show clear T_g and T_x with a wide supercooled liquid region before the onset of crystallization. This proves that the amorphous phase prepared by mechanical alloying is comparable in its structure to that synthesized by liquid metallurgy route. The thermal stability of the amorphous phase in the milled samples is similar to the results reported for melt spun and slowly cooled samples of similar compositions. Fig. 9(b) is an example of the compositions studied, which shows a ΔT_x of 60 °C for $Ti_{50}Cu_{23}Ni_{20}Sn_7$, which is higher than that reported for the same composition by the liquid metallurgy route ($\Delta T_x = 49$ °C) [6]. This suggests that the amorphous phase obtained by MA is more stable than that made by the liquid metallurgy route at least in some compositions.

4. Conclusions

(1) Milling maps/energy maps have been developed for a number of bulk metallic glass forming compositions. The results indicate that the energy required for amorphisation falls in a range of 500–600 J g^{-1} for all the compositions studied.
(2) Amorphisation in all the compositions has been observed below a critical crystallite size of about 20 nm.

Acknowledgements

Authors are thankful to Board of Research in Nuclear Sciences, Department of Atomic Energy, Government of India for the financial support.

References

[1] A. Inoue, Acta Mater. 48 (2000) 279–306.
[2] M.C. Lee, H.J. Fecht, J.L. Allen, J.H. Perepezko, K. Ohsaka, W.L. Johnson, Mater. Sci. Eng. 97 (1988) 301–305.
[3] A.J. Drehman, A.L. Greer, D. Turnbull, Appl. Phys. Lett. 41 (1982) 716–717.
[4] A. Inoue, K. Ohtera, K. Kita, T. Masumoto, Jpn. J. Appl. Phys. 27 (1988) L2248–L2251.
[5] A. Peker, W.L. Johnson, Appl. Phys. Lett. 63 (1993) 2342–2344.
[6] T. Zhang, A. Inoue, Mater. Trans. JIM 39 (1998) 1001–1006.
[7] A. Inoue, T. Zhang, H. Koshiba, A. Makino, J. Appl. Phys. 83 (1998) 6326–6328.
[8] A. Inoue, W. Zhang, T. Zhang, K. Kurosaka, Mater. Trans. JIM 42 (2001) 1149–1151.

[9] W. Zhang, A. Inoue, Scripta Mater. 48 (2003) 641–645.
[10] J. Eckert, Mater. Sci. Eng. A 226–228 (1997) 364–373.
[11] W.L. Johnson, Prog. Mater. Sci. 30 (1986) 81–134.
[12] C.C. Koch, O.B. Cavin, C.G. McKamey, J.O. Scarbrough, Appl. Phys. Lett. 43 (1983) 1017–1019.
[13] B.S. Murty, S. Ranganathan, Int. Mater. Rev. 43 (1998) 101–141.
[14] C. Suryanarayana, Prog. Mater. Sci. 46 (2001) 1–184.
[15] B.S. Murty, M.K. Datta, S.K. Pabi, Sadhana 28 (2003) 23–45.
[16] D.B. Witkin, E.J. Lavernia, Prog. Mater. Sci. 51 (2006) 1–60.
[17] B.S. Murty, M. Mohan Rao, S. Ranganathan, Acta Metall. Mater. 43 (1995) 2443–2450.
[18] J. Joardar, S.K. Pabi, B.S. Murty, J. Alloys Compd. 429 (2007) 204–210.
[19] H. Mio, J. Kanoa, F. Saito, K. Kaneko, Int. J. Miner. Process. 74S (2004) S85–S92.
[20] O. Boytsov, A.I. Ustinov, E. Gaffet, F. Bernard, J. Alloys Compd. 432 (2007) 103–110.
[21] M. Abdellaoui, E. Gaffet, Acta Metall. Mater. 43 (1995) 1087–1098.
[22] M. Magini, C. Colella, A. Iasonna, F. Padella, Acta Mater. 46 (1998) 2841–2850.
[23] N. Burgio, A. Iasonna, M. Magini, S. Martelli, F. Padella, Il Nuovo Cimento 13 (1991) 459–465.
[24] T. Rojac, M. Kosec, B. Malič, J. Holc, J. Eur. Ceram. Soc. 26 (2006) 3711–3716.
[25] C. Suryanarayana, G.-H. Chen, F.H. Froes, Scripta Metall. Mater. 26 (1992) 1727–1732.
[26] A. Guinier, X-Ray Diffraction, Freeman, San Francisco, 1963.
[27] M. Magini, A. Iasonna, F. Padella, Scripta Mater. 34 (1996) 13–19.
[28] Z.P. Lu, C.T. Liu, Acta Mater. 50 (2002) 3501–3512.
[29] K. Mondal, B.S. Murty, J. Non-cryst. Solids 351 (2005) 1366–1371.
[30] B. Srinivasa Rao, J. Bhatt, B.S. Murty, Mater. Sci. Eng. A 449–451 (2007) 211–214.
[31] B.S. Murty, M. Mohan Rao, S. Ranganathan, Mater. Sci. Eng. A 149 (1992) 231–240.